ISSN 2075-1087, Gyroscopy and Navigation, 2024, Vol. 15, No.1, pp. 39-51
Russian Text © The Author(s), 2024, published in Giroskopiya i Navigatsiya, 2024, No.1, pp. 53-71.

Star Tracker Error Model Taking into Account the Calibration Errors of Intrinsic Parameters of the Digital Camera

N. N. Vasilyuk

SPC Elektrooptika, LLC, Moscow, Russia
**e-mail: nik-vasilyuk@yandex.ru*
Received September 12, 2023; reviewed December 20, 2023; accepted December 20, 2023

Abstract: The error model of the star tracker is presented as a decomposition into fluctuation and systematic components. The fluctuation error, which arises in the calculation of the star digital image brightness center coordinates, is due to the discrete structure of the signal in the matrix photodetector. When star observations are performed through the atmosphere, the fluctuation error has an additional external component associated with the "jitter" of star images caused by atmospheric turbulence. The systematic error follows from the calibration errors of the intrinsic parameters of the digital camera. Linearized analytical expressions and covariance matrices that depend on the configuration of the observed constellation are derived for all components of the attitude error. The error model is easy to rewrite as an observation equation for the errors in estimating the camera intrinsic parameters in a tightly-coupled integrated astronavigation system. The results of the experimental verification of the proposed error model are discussed. The numerical error values obtained in the experiment make clear the need for regular calibration of the intrinsic parameters of the star tracker's digital camera during operation.

Keywords: star tracker, error model, centroid, star jitter, distortion calibration, observation equation.

1. INTRODUCTION

Measurement of attitude with a star tracker is based on the comparison of the measured and catalog Cartesian coordinates of unit direction vectors specifying the same star directions (hereinafter referred to as star direction vectors). The measured coordinates of the star direction vectors are calculated from the star field image obtained with a digital camera. The corresponding catalog coordinates are derived based on the star catalog data. Such a comparison is aimed to determine the attitude of the right orthogonal coordinate frame associated with the camera structure relative to the right orthogonal inertial coordinate frame of the star catalog. The star tracker measurements can be referenced to the Earth's surface only with the use of additional information. Thus, if the vertical direction at the observation point is known, the star tracker measurements make it possible to calculate the observer's longitude and latitude, as well as the azimuth of the camera's optical axis. If the geodetic coordinates of the observation point are known, the measurements of the star tracker's attitude (relative to the stars) allow calculating its attitude relative to the Earth's topocentric coordinate frame (heading, roll and pitch angles). The height above the Earth's surface is not calculated from the star tracker measurements [1].

Determination of the best (in the sense of a quadratic target function) attitude parameters from noisy unit-vector coordinates is carried out in terms of Wahba's problem [2]. The QUEST algorithm, representing the solution to Wahba's problem in the form of an attitude quaternion, is widely known [3]. This algorithm does not require significant computing resources and is suitable for real-time implementation. The algorithm for Wahba's problem solution based on singular decomposition shows the best numerical stability [4]. The structure of this algorithm makes it possible to derive some general analytical relations concerning Wahba's problem. Several algorithms for real-time solution of Wahba's problem have been developed to date based on these two approaches. They are adapted to be used both for stand-alone star trackers and those integrated into astronavigation systems [5].

The error in measuring attitude by a star tracker (star tracker error) depends on the errors in measuring the coordinates of individual star direction vectors and the spatial structure of the bundle of vectors. Reference [3] proposes a simple formula for calculating the covariance matrix of a small rotation vector that describes the star tracker error. This formula was ob-

tained under the assumption that the true values of the measured and catalog coordinates of the direction vectors coincide (i.e. for zero rotation). In this work, we use the formula for the covariance matrix of star tracker errors obtained in [4] for an arbitrary rotation. In some works, the covariance matrix of the star tracker error is considered diagonal [6,7], although this is obviously not the case [8].

If we correct the influence of external effects that systematically distort apparent stellar lines [9,10], the errors in measuring star direction vectors inside the star tracker are divided into fluctuation and systematic errors [11,12]. Fluctuation errors are caused by discrete (quantum) noise in the optical signal coming from the star and electronic noise in the path for the optical signal-to-digital code conversion. It has been shown [5] that zero-mean fluctuation errors in the measured vectors do not lead to a bias in the star tracker's attitude measurements in the first-order infinitesimal. It shows itself only in the second- and higher orders infinitesimals.

For a star tracker located inside the Earth's atmosphere, the fluctuation error in measuring direction vectors has an additional component associated with random variations in the apparent direction to the star. The changes are caused by atmospheric turbulence, which leads to local fluctuations in the refractive index of the air along the path of starlight. In a digital image, these changes are manifested as jitter of the star image about some average position. The standard deviation of the star direction vector jitter is 1–3 arcsec, estimated from the solar limb jitter and the results of the star observation in the morning atmosphere [13,14].

The main part of the systematic errors in measuring direction vectors of stars is of a geometric nature. It is associated with the deviation of the actual values of the camera intrinsic parameters (focal length, coordinates of the principal point of the image, geometric distortion factors) from the nominal ones. These deviations are calibrated during both the star tracker manufacturing [15,16] and operation [17–19]. A certain contribution to the systematic error is made by energy distortion [20] (also called microdistortion [21]), which is associated with errors in spatial discretization of the star optical image in a digital camera. Reference [12] considers the influence of the "dark" signal nonuniformity in individual photosensitive cells on the systematic error in determining the direction to the star. The influence of calibration errors of intrinsic parameters on the star tracker's error is not studied in the available literature.

In this paper, we propose a linearized model of the star tracker's errors, which includes a fluctuation component in determining the coordinates of images of individual stars and takes into account the errors in calibration of the camera intrinsic parameters. The fluctuation component combines discrete signal noise in individual pixels of a star digital image and the jitter of this image due to atmospheric turbulence. Calibration errors lead to a bias in the star tracker's attitude measurements even in the first-order infinitesimal. In this case, the bias depends on the shape and angular dimensions of the observed constellation. The developed star tracker error model does not take into account the errors of the models of atmospheric refraction and velocity aberration of light used for computational correction of these effects. The proposed model was tested on experimental data obtained in ground-based calibration of intrinsic parameters of a real digital camera.

2. MODEL OF THE STAR TRACKER PRIMARY MEASUREMENTS

2.1. Geometric model of a digital camera

The digital camera lens of a star tracker forms an optical image of the observed constellation on the surface of a semiconductor matrix photodetector (MPD). The MPD surface is a flat rectangular matrix of size $H \times W$, where H, W are the height and width of the matrix containing homogenous square-shaped photosensitive cells with side length a (Fig. 1).

The position of an individual photosensitive cell in the MPD plane is specified by a pair of integer raster indices $(\hat{h}, \hat{w}) \in \mathbb{Z}^2$, where $\hat{h} = 0 \ldots H-1$, $\hat{w} = 0 \ldots W-1$. The values of indices (0, 0) correspond to the cell located in the MPD upper left corner. Indices $\hat{h}$, $\hat{w}$ increase in the directions from top to bottom and from left to right along the vertical and horizontal sides of the MPD. The continuous optical image formed by the lens on the MPD plane is subject to spatial discretization at the boundaries of individual cells. The signals received by individual cells are converted into digital codes, readout from the MPD, and are arranged in the form of a numerical matrix of size $H \times W$ called a digital image. A pixel with indices $(\hat{h}, \hat{w})$ inside a digital image obtains its value from a photosensitive cell with indices $(\hat{h}, \hat{w})$ inside the MPD matrix.

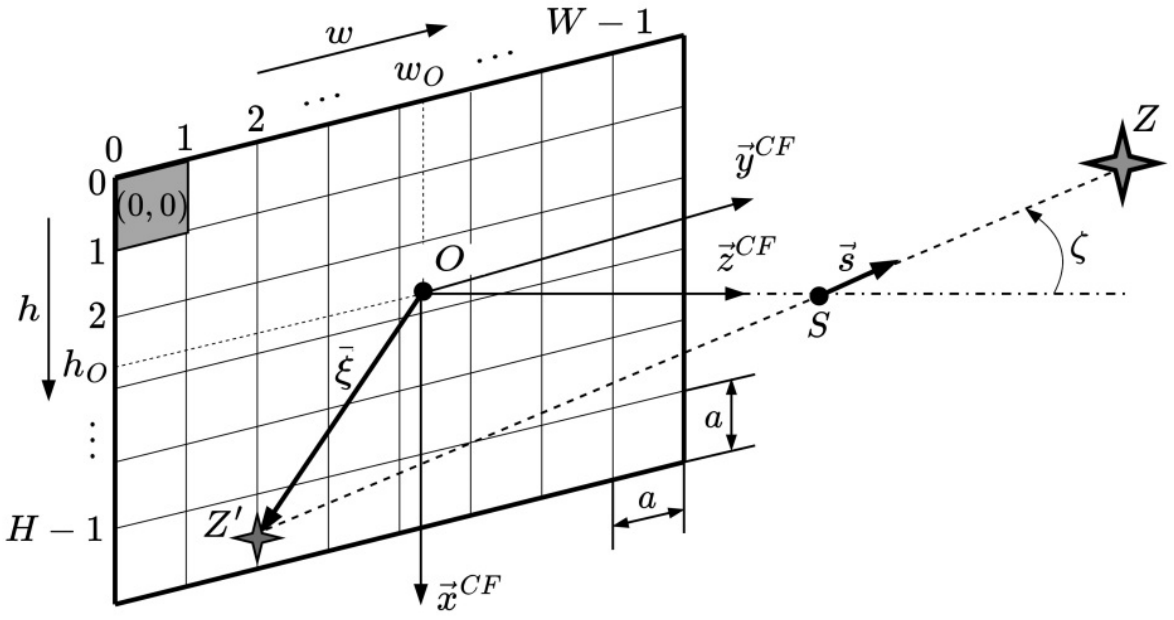

Fig. 1. Geometric model of a digital camera and coordinate frame. The dash-dotted line indicates the optical axis of the camera. The designations used in the figure are explained in the text.

The process of spatial discretization of the image in the MPD plane is described with the use of real-valued raster coordinates $[h\ w]^{\mathsf{T}} \in \mathbb{R}^2$, $0 \le h < H$, $0 \le w < W$ with the origin in the upper left corner of the upper left MPD cell (cells with raster indices $(\hat{h}, \hat{w}) = (0, 0)$). The values of the coordinates *h, w* increase in the direction of growth of the namesake indices $\hat{h}$, $\hat{w}$. The scale of raster coordinates is chosen so that the point on the MPD surface with integer values of raster coordinates $[\hat{h}\ \hat{w}]^{\mathsf{T}}$ falls into the upper left corner of the MPD cell with raster indices $(\hat{h}, \hat{w})$. Thus, the formation of the value in pixel $(\hat{h}, \hat{w})$ involves points of a continuous optical image with raster coordinates $[h\ w]^{\mathsf{T}}$ from a two-dimensional set, which is defined as the Cartesian product of half-intervals $[\hat{h}, \hat{h}+1)\times[\hat{w}, \hat{w}+1)$.

The MPD surface is located in the focal plane of the lens. The optical axis of the lens is perpendicular to the MPD surface, intersecting it at point *O* with raster coordinates $[h_O\ w_O]^{\mathsf{T}}$. Point *O*, called the principal point of the image (not to be confused with the principal point of the lens), lies close to the MPD geometric center. Associated with the digital camera is the right orthonormal coordinate frame *CF* (camera frame), with the origin at point *O*; axis $\vec{z}^{CF}$ lies on the optical axis of the lens and is directed to world space; axes $\vec{x}^{CF}$, $\vec{y}^{CF}$ are parallel to the vertical and horizontal sides of the MPD and directed to increasing raster coordinates *h* and *w*, respectively (Fig. 1).

An ideal lens forms a geometric image of star *Z* as its central projection *Z′* onto the focal plane. The projection center *S* is located on the optical axis of the lens, spaced from the focal plane by the focal length *F* = *OS*. The direction to star *Z* in world space is described by unit direction vector $\vec{s}$ with a coordinate column in *CF* $\mathbf{s}_{CF} = [s_{xCF}\ \ s_{yCF}\ \ s_{zCF}]^{\mathsf{T}}$. The position of point *Z′* in the MPD plane is specified by vector $\vec{\xi}$ with coordinates $\xi = [x\ y]^{\mathsf{T}}$ relative to axes $\vec{x}^{CF}$ and $\vec{y}^{CF}$. Coordinates ξ, called the vector coordinates of image *Z′*, are related to the coordinates **s** of the star *Z* direction vector by the following formulas:

$$\xi = -\frac{F}{s_{zCF}}\begin{bmatrix} s_{xCF} \\ s_{yCF} \end{bmatrix},\ \mathbf{s} = \frac{[-x\ \ -y\ \ F]^{\mathsf{T}}}{(x^2 + y^2 + F^2)^{1/2}}. \qquad (1)$$

Vector ξ and raster $[h\ w]^{\mathsf{T}}$ coordinates of the representing point *Z′* are related by the formulas

$$\xi = a\begin{bmatrix} h - h_O \\ w - w_O \end{bmatrix},\ \begin{bmatrix} h \\ w \end{bmatrix} = \frac{\xi}{a} + \begin{bmatrix} h_O \\ w_O \end{bmatrix}. \qquad (2)$$

The geometric image formed by a real lens deviates from the central projection. This deviation is called geometric distortion and is described by the Brown-Conrady model, well known in the photogrammetric literature [22, 23]. Within this model, distortion is divided into radial and tangential distortions. Radial distortion appears on the spherical surfaces of successive lenses with coinciding axes of symmetry. Tangential distortion is caused by errors in the posi-

tion of individual lenses along the common axis of symmetry. The star tracker digital camera is a measurement device for which radial distortion is predominant due to the sphericity of the lens surfaces rather than errors in the lens assembly.

Let $\boldsymbol{\eta} = [\tilde{x}\ \ \tilde{y}]^{\mathrm{T}}$ be the vector coordinates of the geometric image of the star formed by a lens with distortion. In these coordinates, the radial distortion is corrected as follows:

$$\boldsymbol{\xi} = (1 + k_1\,\tilde{r}^2 + k_2\,\tilde{r}^4 + ...)\boldsymbol{\eta}, \qquad (3)$$

where $\tilde{r}^2 = \boldsymbol{\eta}^{\mathrm{T}}\boldsymbol{\eta}$; $k_1, k_2, \ldots$ are radial distortion coefficients. At the principal point of the image, $x = \tilde{x} = y = \tilde{y} = 0$, therefore, $\boldsymbol{\xi} = \boldsymbol{\eta}$, i.e. there is no radial distortion at this point.

For second-order distortion, the transformation of the plane coordinates of the star image into the spatial coordinates of its direction vector is described by vector $\mathbf{p} = [F\ \ h_O\ \ w_O\ \ k_1\ \ k_2]^{\mathrm{T}}$ consisting of five parameters, called intrinsic parameters of the camera. Their true values are determined as a result of manufacturing calibration and later refined during the star tracker operation.

1.2. Measuring star image coordinates

The lens of a stationary star tracker forms a star image as a diffuse spot. The illumination distribution of this spot is described by the point spread function (PSF). The coordinates of the spot's digital image center are measured by superposition of a square averaging window of $2N_W+1 \times 2N_W+1$ pixels on it, where $N_W \in \mathbb{N}$ is the window half-width. The raster coordinates of the center of mass (also called the brightness center or photocenter of the spot) of all pixels within the averaging window are considered to be measured coordinates [12, 24]:

$$\tilde{h}_S = \frac{1}{I_\Sigma}\sum_{\hat{h}=\hat{h}_C-N_W}^{\hat{h}_C+N_W}\hat{h}\sum_{\hat{w}=\hat{w}_C-N_W}^{\hat{w}_C+N_W} I(\hat{h},\hat{w}),$$

$$\tilde{w}_S = \frac{1}{I_\Sigma}\sum_{\hat{w}=\hat{w}_C-N_W}^{\hat{w}_C+N_W}\hat{w}\sum_{\hat{h}=\hat{h}_C-N_W}^{\hat{h}_C+N_W} I(\hat{h},\hat{w}), \qquad (4)$$

$$I_\Sigma = \sum_{\hat{w}=\hat{w}_C-N_W}^{\hat{w}_C+N_W}\sum_{\hat{h}=\hat{h}_C-N_W}^{\hat{h}_C+N_W} I(\hat{h},\hat{w}),$$

where $(\hat{h}_C, \hat{w}_C)$ are raster indices of the pixel in which the window center lies; $I(\hat{h},\hat{w}) = I_{raw}(\hat{h},\hat{w}) - \langle I_{bg}(\hat{h},\hat{w})\rangle$ is the brightness of pixel $(\hat{h},\hat{w})$ with expected value $\langle I(\hat{h},\hat{w})\rangle$ after the background subtraction; $I_{raw}(\hat{h},\hat{w})$ is the raw brightness of pixel $(\hat{h},\hat{w})$ obtained from the MPD; $\langle I_{bg}(\hat{h},\hat{w})\rangle$ is the expected value of the background level. Coordinates $[\tilde{h}_S\ \ \tilde{w}_S]^{\mathrm{T}}$ are distorted.

The background level $I_{bg}(\hat{h},\hat{w})$ is an additive signal generated by the radiation of the background against which the star is observed and by all kinds of internal MPD currents. The values of $\langle I_{bg}(\hat{h},\hat{w})\rangle$ are calculated directly from the frame being processed. Further, methodological errors in the $\langle I_{bg}(\hat{h},\hat{w})\rangle$ calculation are not taken into account, that is, after $\langle I_{bg}(\hat{h},\hat{w})\rangle$ is subtracted, brightness $I(\hat{h},\hat{w})$ comprises only the fluctuation component of the background, and $\langle I(\hat{h},\hat{w})\rangle$ contains only the expected value of the useful signal.

Fluctuations $\delta I(\hat{h},\hat{w}) = I(\hat{h},\hat{w}) - \langle I(\hat{h},\hat{w})\rangle$ in individual pixels are considered independent and the expected values of the "measured" raster coordinates of the star are described by the following formulas:

$$\langle\tilde{h}_S\rangle \approx \frac{1}{\langle I_\Sigma\rangle}\sum_{\hat{h}=\hat{h}_C-N_W}^{\hat{h}_C+N_W}\hat{h}\sum_{\hat{w}=\hat{w}_C-N_W}^{\hat{w}_C+N_W}\langle I(\hat{h},\hat{w})\rangle,$$

$$\langle\tilde{w}_S\rangle \approx \frac{1}{\langle I_\Sigma\rangle}\sum_{\hat{w}=\hat{w}_C-N_W}^{\hat{w}_C+N_W}\hat{w}\sum_{\hat{h}=\hat{h}_C-N_W}^{\hat{h}_C+N_W}\langle I(\hat{h},\hat{w})\rangle,$$

$$\langle I_\Sigma\rangle = \sum_{\hat{w}=\hat{w}_C-N_W}^{\hat{w}_C+N_W}\sum_{\hat{h}=\hat{h}_C-N_W}^{\hat{h}_C+N_W}\langle I(\hat{h},\hat{w})\rangle.$$

Here, sign "≈" indicates that they are valid only for the first-order $\delta I(\hat{h},\hat{w})$. When higher-order variations are taken into account, the estimates of the expected values may have biases [25]. Fluctuations in brightness cause errors in the calculations of the brightness center coordinates:

$$\delta\tilde{h}_S = \tilde{h}_S - \langle\tilde{h}_S\rangle = \frac{1}{\langle I_\Sigma\rangle}\sum_{\hat{h}=\hat{h}_C-N_W}^{\hat{h}_C+N_W}\Delta\tilde{h}_S\sum_{\hat{w}=\hat{w}_C-N_W}^{\hat{w}_C+N_W}\delta I(\hat{h},\hat{w}),$$

$$\delta\tilde{w}_S = \tilde{w}_S - \langle\tilde{w}_S\rangle = \frac{1}{\langle I_\Sigma\rangle}\sum_{\hat{w}=\hat{w}_C-N_W}^{\hat{w}_C+N_W}\Delta\tilde{w}_S\sum_{\hat{h}=\hat{h}_C-N_W}^{\hat{h}_C+N_W}\delta I(\hat{h},\hat{w}),$$

where $\Delta\tilde{h}_S = \hat{h} - \langle\tilde{h}_S\rangle$, $\Delta\tilde{w}_S = \hat{w} - \langle\tilde{w}_S\rangle$. The covariance matrix of these errors takes the form:

$$\mathrm{cov}\{[\delta\tilde{h}_S\ \ \delta\tilde{w}_S]^{\mathrm{T}}\} = \begin{bmatrix}\sigma_{hh}^2 & \sigma_{hw}^2\\ \sigma_{hw}^2 & \sigma_{ww}^2\end{bmatrix}, \qquad (5)$$

where $\sigma_{hh}^2 = \frac{1}{\langle I_\Sigma\rangle^2}\sum_{\hat{h}=\hat{h}_C-N_W}^{\hat{h}_C+N_W}\Delta\tilde{h}_S^2\sum_{\hat{w}=\hat{w}_C-N_W}^{\hat{w}_C+N_W}\sigma_I^2(\hat{h},\hat{w})$,

$$\sigma_{ww}^2 = \frac{1}{\langle I_\Sigma \rangle} \sum_{\hat{w}=\hat{w}_C-N_W}^{\hat{w}_C+N_W} \Delta\tilde{w}_S^2 \sum_{\hat{h}=\hat{h}_C-N_W}^{\hat{h}_C+N_W} \sigma_I^2(\hat{h},\hat{w}),$$

$$\sigma_{hw}^2 = \frac{1}{\langle I_\Sigma \rangle} \sum_{\hat{w}=\hat{w}_C-N_W}^{\hat{w}_C+N_W} \sum_{\hat{h}=\hat{h}_C-N_W}^{\hat{h}_C+N_W} \Delta\tilde{w}_S \Delta\tilde{h}_S \, \sigma_I^2(\hat{h},\hat{w}),$$

$$\sigma_I^2(\hat{h},\hat{w}) = \langle \delta I(\hat{h},\hat{w})^2 \rangle .$$

The simplest variant of the PSF approximation is the axisymmetric Gaussian function of vector coordinates with a maximum at point Z' [26]:

$$\Phi(x,y) = \frac{1}{2\pi\sigma_A^2} \exp\left(-\frac{x^2+y^2}{2\sigma_A^2} \right),$$

where $\sigma_A = r_A / \sqrt{-2\ln(1-A)}$ is the parameter of the circle of confusion (CoC); r_A is the radius of the CoC into which fraction $0 < A < 1$ of the radiation flux from the star falls [27]. Next, we consider a circle inscribed in a 2×2 cluster of adjacent photosensitive cells, i.e. $r_A = a$, at the boundary of which (on the circle $x^2 + y^2 = r_A^2$) the PSF value decreases by a factor of e^2 relative to its maximum. For this circle, with parameters $r_A = a = 2\sigma_A$, $\sigma_A = 0.5a$, $A \approx 0.865$, the simulation in [21,24] shows that calculated by (4), the maximum systematic error in determining raster coordinates of the star geometric image (point Z' in Fig. 1) does not exceed $0.05a$. For further calculations, we neglect this error and assume that Z' lies exactly in the center of cell ($\hat{h}_C$, $\hat{w}_C$), and its raster coordinates are given as $[\hat{h}_C + \delta h \;\; \hat{w}_C + \delta w]^\mathsf{T}$, $\delta h = \delta w = 0.5$. In this case, the systematic error (4) is zero.

The expected value of signal $\langle I(\hat{h},\hat{w}) \rangle$ in cell $(\hat{h},\hat{w}) = (\hat{h}_C+\hat{p}, \hat{w}_C+\hat{q})$, $\hat{p},\hat{q} = -N_W \ldots N_W$ within the window is proportional to the number of electrons accumulated in the charge well of the cell:

$$\langle I(\hat{h}_C+\hat{p}, \hat{w}_C+\hat{q}) \rangle = kN_\mathrm{e} \, \hat{\Phi}(\hat{p},\hat{q}),$$

$$\hat{\Phi}(\hat{p},\hat{q}) = \int_{a(\hat{p}-\delta h)}^{a(\hat{p}+1-\delta h)} dx \int_{a(\hat{q}-\delta w)}^{a(\hat{q}+1-\delta w)} dy \, \Phi(x,y), \qquad (6)$$

where $N_\mathrm{e} = P_\mathrm{e} T_E$ is the expected value of the total number of electrons accumulated in all MPD cells illuminated by starlight during exposure time T_E; P_e is the power of stellar radiation incident on the MPD surface expressed through the rate of photoelectron production in the MPD semiconductor structure; k is the proportionality coefficient converting the number of electrons into units of the least significant digit of the ADC [28]. The P_e value is calculated for each star for the built-in star catalog of the star tracker based on the star radiation spectrum, the energy characteristics of the digital camera lens, and the spectral distribution of the MPD quantum efficiency [29,30]. In (6), the cos ζ factor was omitted, where ζ is the angle between the direction to the star and the optical axis of the camera (Fig. 1). The field of view of navigation star trackers does not exceed 30°, i.e. $\cos\zeta \geq \cos 15° \approx 0.966$. Without compromising the accuracy of the model under consideration, this factor can be set equal to 1. The formula for the coefficients $\hat{\Phi}(\hat{p},\hat{q})$ of the spatially discretized PSF is written using the standard Gaussian error function erf(x) [24]:

$$\hat{\Phi}(\hat{p},\hat{q}) = \frac{1}{4}\left[\mathrm{erf}\left(\frac{a(\hat{p}+1-\delta h)}{\sqrt{\alpha}} \right) - \mathrm{erf}\left(\frac{a(\hat{p}-\delta h)}{\sqrt{\alpha}} \right) \right] \times$$

$$\times \left[\mathrm{erf}\left(\frac{a(\hat{q}+1-\delta w)}{\sqrt{\alpha}} \right) - \mathrm{erf}\left(\frac{a(\hat{q}-\delta w)}{\sqrt{\alpha}} \right) \right],$$

where $\alpha = 2\sigma_A^2 \approx 0.5a^2$, $\delta h = \delta w = 0.5$; $\mathrm{erf}(x) = \frac{2}{\sqrt{\pi}} \int_0^x e^{-t^2} \, dt$. The derivation of this expression is given in Appendix.

The brightness dispersion $\sigma_I^2(\hat{h}_C+\hat{p}, \hat{w}_C+\hat{q}) \equiv \sigma_I^2(\hat{p},\hat{q}) = \sigma_Q^2(\hat{p},\hat{q}) + k^2\sigma_{bg}^2$ comprises dispersion $\sigma_Q^2(\hat{p},\hat{q})$ of the quantum noise of the signal from the star and dispersion σ_{bg}^2 of the background fluctuation component. Quantum noise has the Poisson distribution, and its dispersion takes the form

$$\sigma_Q^2(\hat{p},\hat{q}) = k^2 N_\mathrm{e} \hat{\Phi}(\hat{p},\hat{q}) = k \langle I(\hat{h}_C+\hat{p}, \hat{w}_C+\hat{q}) \rangle .$$

Dispersion $\sigma_{bg}^2 = \sigma_{rd}^2 + \sigma_{dc}^2 + \sigma_{ob}^2 + \sigma_{ADC}^2$, where σ_{rd}^2 is the dispersion of the readout noise; $\sigma_{dc}^2 = i_{dc} T_E$ is dark charge dispersion, i_{dc} is the MPD dark current; σ_{ob}^2 is Poisson dispersion of optical background radiation; $\sigma_{ADC}^2 = QS^2/12$ is quantization noise dispersion, QS is a quantization step. The values of σ_{rd}, i_{dc} and QS are given in the MPD specification, and σ_{ob} is calculated based on observation conditions. An example of such a calculation is given below.

Now we can rewrite the coefficients of the covariance matrix (5):

$$\sigma_{hh}^2 = \frac{1}{N_\mathrm{e}} \sum_{\hat{p}=-N_W}^{N_W} \sum_{\hat{q}=-N_W}^{N_W} \frac{(\hat{p}-\delta h)^2 \hat{\Phi}(\hat{p},\hat{q})}{\hat{\Phi}_\Sigma^2} +$$

$$+ \frac{\sigma_{bg}^2}{N_\mathrm{e}^2} \sum_{\hat{q}=-N_W}^{N_W} \sum_{\hat{p}=-N_W}^{N_W} \frac{(\hat{p}-\delta h)^2}{\hat{\Phi}_\Sigma^2},$$

$$\sigma_{ww}^2 = \frac{1}{N_e}\sum_{\hat{q}=-N_W}^{N_W}\sum_{\hat{p}=-N_W}^{N_W}\frac{(\hat{q}-\delta w)^2\hat{\Phi}(\hat{p},\hat{q})}{\hat{\Phi}_\Sigma^2} + \\ + \frac{\sigma_{bg}^2}{N_e^2}\sum_{\hat{p}=-N_W}^{N_W}\sum_{\hat{q}=-N_W}^{N_W}\frac{(\hat{q}-\delta w)^2}{\hat{\Phi}_\Sigma^2},$$

$$\sigma_{hw}^2 = \frac{1}{N_e}\sum_{\hat{q}=-N_W}^{N_W}\sum_{\hat{p}=-N_W}^{N_W}\frac{(\hat{q}-\delta w)(\hat{p}-\delta h)\hat{\Phi}(\hat{p},\hat{q})}{\hat{\Phi}_\Sigma^2} + \\ + \frac{\sigma_{bg}^2}{N_e^2}\sum_{\hat{q}=-N_W}^{N_W}\sum_{\hat{p}=-N_W}^{N_W}\frac{(\hat{q}-\delta w)(\hat{p}-\delta h)}{\hat{\Phi}_\Sigma^2},$$

$$\hat{\Phi}_\Sigma = \sum_{\hat{q}=-N_W}^{N_W}\sum_{\hat{p}=-N_W}^{N_W}\hat{\Phi}(\hat{p},\hat{q}).$$

The typical window size for the CoC with $r_A = a$ is 3×3 pixels, i.e. $N_W = 1$ [12]. For this case, the covariance matrix of the random error in determining the raster coordinates of the brightness center takes the form:

$$\mathrm{cov}\{[\delta\tilde{h}_S \;\; \delta\tilde{w}_S]^\mathsf{T}\} = \\ = \frac{1}{P_e T_E}\begin{bmatrix}0.5682 & 0.2513\\ 0.2513 & 0.5682\end{bmatrix} + \frac{\sigma_{bg}^2}{(P_e T_E)^2}\begin{bmatrix}8.3391 & 2.2743\\ 2.2743 & 8.3391\end{bmatrix}.$$

Formula (3) for distortion correction can be rewritten with $\mathbf{H} = \boldsymbol{\eta}\boldsymbol{\eta}^\mathsf{T}$:

$$\boldsymbol{\xi} = (1 + k_1\boldsymbol{\eta}^\mathsf{T}\boldsymbol{\eta} + k_2(\boldsymbol{\eta}^\mathsf{T}\boldsymbol{\eta})^2)\boldsymbol{\eta} = (\mathbf{I}_2 + k_1\mathbf{H} + k_2\mathbf{H}^2)\boldsymbol{\eta},$$

where $\boldsymbol{\eta} = a[\tilde{h}_S - h_O \;\; \tilde{w}_S - w_O]^\mathsf{T}$ are the vector coordinates of the star image brightness center before distortion correction, calculated according to (2). This expression is varied to derive an error in the vector coordinates of the brightness center after distortion correction:

$$\delta\boldsymbol{\xi}_{dst} = (\delta k_1\mathbf{H} + \delta k_2\mathbf{H}^2)\boldsymbol{\eta} + (k_1\delta\mathbf{H} + k_2[\delta\mathbf{H}\,\mathbf{H} + \mathbf{H}\,\delta\mathbf{H}])\boldsymbol{\eta} + \\ + (\mathbf{I}_2 + k_1\mathbf{H} + k_2\mathbf{H}^2)\delta\boldsymbol{\eta},$$

where $\delta\boldsymbol{\eta} = \delta\boldsymbol{\eta}_{ns} - a[\delta\tilde{h}_S \;\; \delta\tilde{w}_S]^\mathsf{T}$ is the vector coordinates error $\boldsymbol{\eta}$, which comprises the fluctuation $\delta\boldsymbol{\eta}_{ns} = a[\delta\tilde{h}_S \;\; \delta\tilde{w}_S]^\mathsf{T}$ and systematic $a[\delta h_O \;\; \delta w_O]^\mathsf{T}$ components arising due to the errors in the calibration of the intrinsic parameters. After rearrangement of the variations, the new expression for $\delta\boldsymbol{\xi}_{dst}$ takes the form:

$$\delta\boldsymbol{\xi}_{dst} = (\mathbf{I}_2 + \mathbf{C}_1)\delta\boldsymbol{\eta}_{ns} - a(\mathbf{I}_2 + \mathbf{C}_1)\begin{bmatrix}\delta h_O\\ \delta w_O\end{bmatrix} + \mathbf{C}_2\begin{bmatrix}\delta k_1\\ \delta k_2\end{bmatrix}, \quad (7)$$

where $\mathbf{C}_1 = k_1(\mathbf{H} + \mathbf{M}) + k_2(\mathbf{H}^2 + \mathbf{M}^2)$, $\mathbf{M} = \tilde{r}^2\mathbf{I}_2 + \mathbf{H}$, $\mathbf{C}_2 = \boldsymbol{\eta}[\tilde{r}^2 \;\; \tilde{r}^4]$. The covariance matrix of the fluctuation component of error $\delta\boldsymbol{\xi}_{dst}$ has the form:

$$\mathbf{P}_{ns} = a^2(\mathbf{I}_2 + \mathbf{C}_1)\,\mathrm{cov}\{[\delta\tilde{h}_S \;\; \delta\tilde{w}_S]^\mathsf{T}\}(\mathbf{I}_2 + \mathbf{C}_1)^\mathsf{T}.$$

2.3. Measuring the direction vector coordinates

The true directions to the stars observed by the star tracker are concentrated around the optical axis of the digital camera along which axis $\vec{z}^{CF}$ is directed; therefore, the method for determining the angular coordinates of the direction to the star in *CF* must be chosen so that in the sequence of two rotations that bring $\vec{z}^{CF}$ to the star direction, there is no rotation about axis $\vec{z}^{CF}$ itself. This choice of sequence of rotations guarantees the absence of singularity in the angular coordinates of the observed star. In what follows, we use the following system of two rotations: the first rotation is about axis $\vec{y}^{CF}$ by an angle φ_y until axis $\vec{z}^{CF}$ is aligned with the projection of the star direction vector onto the plane $\vec{x}^{CF}O\vec{z}^{CF}$. The second rotation is performed by angle φ_x about the axis to which axis $\vec{x}^{CF}$ was brought after the first rotation, until axis $\vec{z}'$ (axis $\vec{z}^{CF}$ was brought into it) is aligned with the direction vector of the star. In this sequence of rotations, the coordinates of the star direction vector $\mathbf{s}_{CF}$ are written as follows:

$$\mathbf{s}_{CF} = [s_{xCF} \;\; s_{yCF} \;\; s_{zCF}]^\mathsf{T} = [s_{\varphi_y}c_{\varphi_x} \;\; -s_{\varphi_x} \;\; c_{\varphi_y}c_{\varphi_x}]^\mathsf{T},$$

where $c_\varphi \equiv \cos\varphi$, $s_\varphi = \sin\varphi$.

Fluctuations $\delta\boldsymbol{\varphi} = [\delta\varphi_y \;\; \delta\varphi_x]^\mathsf{T}$ of the angular coordinates of the direction vector shift its end along two mutually perpendicular directions lying in the plane perpendicular to the true direction to the star. It is further assumed that these fluctuations are independent and have identical normal distributions with zero mean. The numerical values of the standard deviation σ_{sh} of model fluctuations $\delta\varphi_y$, $\delta\varphi_x$ are calculated from the experimental value of the standard deviation of the solar limb angular jitter equal to 3arcsec [13,14]: $(\langle\delta\varphi_x^2\rangle + \langle\delta\varphi_y^2\rangle)^{1/2} = \sqrt{2\sigma_{sh}^2} = 3$ arcsec, whence $\sigma_{sh} = 2.1$ arcsec. Turbulent fluctuations $\delta\mathbf{t}_{CF}$ of the direction vector coordinates $\mathbf{s}_{CF}$, $\delta\mathbf{t}_{CF} \perp \mathbf{s}_{CF}$ can be written as

$$\delta\mathbf{t}_{CF} = \begin{bmatrix}c_{\varphi_y}c_{\varphi_x} & -s_{\varphi_y}s_{\varphi_x}\\ 0 & -c_{\varphi_x}\\ -s_{\varphi_y}c_{\varphi_x} & -c_{\varphi_y}s_{\varphi_x}\end{bmatrix}\delta\boldsymbol{\varphi} = \\ = \begin{bmatrix}s_{zCF} & s_{xCF}s_{yCF}/(1-s_{yCF}^2)^{1/2}\\ 0 & -(1-s_{yCF}^2)^{1/2}\\ -s_{xCF} & s_{zCF}s_{yCF}/(1-s_{yCF}^2)^{1/2}\end{bmatrix}\delta\boldsymbol{\varphi}.$$

The vector coordinates ξ of the star image without distortion are related to its direction vector by (1), from which turbulent fluctuations of the vector coordinates are obtained:

$$\delta\boldsymbol{\xi}_{trb} = \frac{F}{s_{zCF}}\begin{bmatrix} -1 & 0 & s_{xCF}/s_{zCF} \\ 0 & -1 & s_{yCF}/s_{zCF} \end{bmatrix}\delta\mathbf{t}_{CF} =$$

$$= \frac{F}{s_{zCF}}\begin{bmatrix} -(1-s_{yCF}^2)/s_{zCF} & 0 \\ -s_{xCF}s_{yCF}/s_{zCF} & (1-s_{yCF}^2)^{-1/2} \end{bmatrix}\delta\boldsymbol{\varphi}.$$

After (1) is substituted to this formula, we derive the final expression for turbulent fluctuations of the star image vector coordinates:

$$\delta\boldsymbol{\xi}_{trb} = \mathbf{T}\,\delta\boldsymbol{\varphi},$$

$$\mathbf{T} = \begin{bmatrix} -(x^2+F^2)/F & 0 \\ -xy/F & (x^2+y^2+F^2)/(x^2+F^2)^{1/2} \end{bmatrix}, \quad (8)$$

where $\mathbf{T}$ is the distribution matrix of turbulent fluctuations of the direction vector angular coordinates in the vector coordinates of the star brightness center. The covariance matrix of turbulent fluctuations has the form:

$$\mathbf{P}_{trb} = \langle \delta\boldsymbol{\xi}_{trb}\delta\boldsymbol{\xi}_{trb}^{\mathsf{T}} \rangle = \sigma_{sh}^2\mathbf{T}\mathbf{T}^{\mathsf{T}}.$$

Variation (1) over all variables leads to the error in determining the star direction vector coordinates from its digital image:

$$\delta\mathbf{s}_{CF} = \frac{\mathbf{I}_3 - \mathbf{s}_{CF}(\mathbf{s}_{CF})^{\mathsf{T}}}{((x^n)^2+(y^n)^2+F^2)^{1/2}}\begin{bmatrix} -\delta\xi \\ \delta F \end{bmatrix}, \ \delta\mathbf{s}_{CF}^n \perp \mathbf{s}_{CF}^n,$$

where $\delta\xi = \delta\xi_{trb} + \delta\xi_{dst}$ is the fluctuation error in determining vector coordinates ξ of the star brightness center after correction for distortion. We substitute (7) and (8) into the formula:

$$\begin{bmatrix} -\delta\xi \\ \delta F \end{bmatrix} = \mathbf{G}_1\delta\boldsymbol{\eta}_{ns} + \mathbf{G}_2\delta\boldsymbol{\varphi} + \mathbf{G}_3\delta\mathbf{p},$$

where $\mathbf{G}_1 = -\begin{bmatrix} \mathbf{I}_2 + \mathbf{C}_1 \\ 0 \quad 0 \end{bmatrix}$, $\mathbf{G}_2 = \begin{bmatrix} -\mathbf{T} \\ 0 \quad 0 \end{bmatrix}$,

$$\mathbf{G}_3 = \left[\begin{array}{c|c|c} 0 & a(\mathbf{I}_2 + \mathbf{C}_1) & -\mathbf{C}_2 \\ 0 & & \\ \hline 1 & 0 \quad 0 & 0 \quad 0 \end{array}\right];$$

$\delta\mathbf{p} = \mathbf{p} - \breve{\mathbf{p}} = [\delta F\ \delta h_O\ \delta w_O\ \delta k_1\ \delta k_2]^{\mathsf{T}}$ are the errors in calibration of the intrinsic parameters; $\breve{\mathbf{p}}$ is the true vector, $\mathbf{p}$ is the calibrated vector used in the star tracker algorithms. The final expression for the fluctuation error of the direction vector of the detected star takes the following form:

$$\delta\mathbf{s}_{CF} = \frac{\mathbf{I}_3 - \mathbf{s}_{CF}(\mathbf{s}_{CF})^{\mathsf{T}}}{(x^2+y^2+F^2)^{1/2}}(\mathbf{G}_1\boldsymbol{\varepsilon} + \mathbf{G}_2\delta\boldsymbol{\varphi} + \mathbf{G}_3\delta\mathbf{p}). \quad (9)$$

3. STAR TRACKER ATTITUDE MEASUREMENT MODEL

Assume that the image obtained by the star tracker's digital camera contains N_S individual stars, and coordinates $\{\mathbf{s}_{CF}^n\}_{n=1}^{N_S}$ of their unit direction vectors are calculated. All these stars are identified, i.e. each star numbered $n = 1...\ N_S$ has a corresponding star catalog's entry that is assigned the same number n. These records were used to calculate coordinates $\{\mathbf{g}_{GCRS}^n\}_{n=1}^{N_S}$ of the unit direction vectors of the same stars, but relative to the inertial geocentric celestial coordinate system (GCRS). Wahba's problem for the two sets of coordinates, $\{\mathbf{g}_{GCRS}^n\}_{n=1}^{N_S}$ and $\{\mathbf{s}_{CF}^n\}_{n=1}^{N_S}$, of the same bundle of vectors is called the problem of finding orthogonal matrix $\mathbf{S}_{CF}^{GCRS}$, for which the target function

$$L(\mathbf{S}_{CF}^{GCRS}) = 0{,}5\sum_{n=1}^{N_S}\nu_n\,|\,\mathbf{s}_{CF}^n - \mathbf{S}_{CF}^{GCRS}\mathbf{g}_{GCRS}^n\,|^2, \ \sum_{n=1}^{N_S}\nu_n = 1$$

reaches its minimum value. Here, $\nu_n > 0$ are the weights of individual measurements which are further assumed to be equal, $\nu_n = 1/N_S$.

To solve this problem, we introduce an intermediate 3×3 matrix $\mathbf{B}$, which is subjected to singular decomposition [4]:

$$\mathbf{B} = \frac{1}{N_S}\sum_{n=1}^{N_S}\mathbf{s}_{CF}^n(\mathbf{g}_{GCRS}^n)^{\mathsf{T}} = \mathbf{U}\boldsymbol{\Lambda}\mathbf{V}^{\mathsf{T}} = \mathbf{U}_+\boldsymbol{\Lambda}'\mathbf{V}_+^{\mathsf{T}},$$

where $\mathbf{U}$, $\mathbf{V}$ are orthogonal matrices of size 3×3; $\boldsymbol{\Lambda} = \mathrm{diag}(\lambda_1, \lambda_2, \lambda_3)$ is a 3×3 diagonal matrix with non-negative singular numbers $\lambda_1 \geq \lambda_2 \geq \lambda_3 \geq 0$; $\mathbf{U}_+ = \mathbf{U}\,\mathrm{diag}(1, 1, \det(\mathbf{U}))$, $\boldsymbol{\Lambda}' = \mathrm{diag}(\lambda_1, \lambda_2, d\lambda_3)$, $\mathbf{V}_+ = \mathbf{V}\,\mathrm{diag}(1, 1, \det(\mathbf{V}))$; $d = \det(\mathbf{U})\det(\mathbf{V}) = \pm 1$ on its main diagonal. The solution to Wahba's problem is matrix

$$\mathbf{S}_{CF}^{GCRS} = \mathbf{U}_+\mathbf{V}_+^{\mathsf{T}} = \mathbf{U}\,\mathrm{diag}(1, 1, d)\,\mathbf{V}^{\mathsf{T}} \approx (\mathbf{I}_3 - [\boldsymbol{\theta}\times])\breve{\mathbf{S}}_{CF}^{GCRS},$$

where $\breve{\mathbf{S}}_{CF}^{GCRS}$ is a true attitude matrix of the star tracker; $\boldsymbol{\theta} = [\theta_x\ \theta_y\ \theta_z]^{\mathsf{T}}$ is the vector of the star tracker small errors; $[\boldsymbol{\theta}\times]$ is a skew-symmetric vector multiplication matrix $\boldsymbol{\theta}\times\mathbf{b} = [\boldsymbol{\theta}\times]\mathbf{b}$:

$$[\boldsymbol{\theta}\times] = \begin{bmatrix} 0 & -\theta_z & \theta_y \\ \theta_z & 0 & -\theta_x \\ -\theta_y & \theta_x & 0 \end{bmatrix}.$$

To strictly calculate the value of $\boldsymbol{\theta}$, we need to know the true values of the catalog $\{\breve{\mathbf{g}}_{GCRS}^n\}_{n=1}^{N_S}$ and observed $\{\breve{\mathbf{s}}_{CF}^n\}_{n=1}^{N_S}$ coordinates. Since these values are unknown, the estimate of vector $\boldsymbol{\theta}$ is calculated further

by substituting the calculated $\{\mathbf{g}^n_{GCRS}\}_{n=1}^{N_S}$ and measured $\{\mathbf{s}^n_{CF}\}_{n=1}^{N_S}$ coordinates into formula [4(33)]:

$$\boldsymbol{\theta} = \mathbf{K}\sum_{n=1}^{N_S}[\mathbf{s}^n_{CF}\times](\mathbf{S}^{GCRS}_{CF}\delta\mathbf{g}^n_{GCRS} - \delta\mathbf{s}^n_{CF}),$$

where $\delta\mathbf{g}^n_{GCRS} = \mathbf{g}^n_{GCRS} - \breve{\mathbf{g}}^n_{GCRS}$ is the error in calculating the catalog coordinates; $\delta\mathbf{s}^n_{CF} = \mathbf{s}^n_{CF} - \breve{\mathbf{s}}^n_{CF}$ is the observation error; $\mathbf{D}$=diag$\left(\lambda_2 + d\lambda_3, \lambda_1 + d\lambda_3, \lambda_1 + \lambda_2\right)$; $\mathbf{K} = (\mathbf{U}_+\mathbf{D}^{-1}\mathbf{U}_+^{\mathsf{T}})/N_S$ is the matrix coefficient of size 3x3.

In modern stellar catalogs, star coordinates are given in the inertial barycentric celestial reference system (BCRS) with the origin at the center of mass of the Solar system [31]. Error $\delta\mathbf{g}^n_{GCRS}$ includes errors in table values of star coordinates in BCRS and errors in converting the direction vector from BCRS to GCRS. The error of the table values does not exceed 0.01arcsec. The error in converting the vector between reference systems comprises errors in taking into account the relativistic aberration from the star tracker's motion and the annual parallax of stars. The aberration can be decomposed into two components––from the orbital motion of the Earth and from the daily rotation of the Earth. The first component is quite significant; it can reach 20 arcsec and is necessarily taken into account during transformation of coordinates. The second component of aberration and annual parallax jointly give an error in coordinate transformation of no more than 1 arcsec, so that it can be neglected [9]. As a result, the final formula for the star tracker error takes the form:

$$\boldsymbol{\theta} = -\mathbf{K}\sum_{n=1}^{N_S}[\mathbf{s}^n_{CF}\times]\delta\mathbf{s}^n_{CF}. \qquad (10)$$

The total error of the star tracker is derived by substituting (9) into (10) and is decomposed into fluctuation component $\boldsymbol{\varepsilon}$ and systematic bias $\mathbf{b}$ of the star tracker:

$$\boldsymbol{\theta} = \boldsymbol{\varepsilon} + \mathbf{b}, \qquad (11)$$

where

$$\boldsymbol{\varepsilon} = -\mathbf{K}\sum_{n=1}^{N_S}\frac{[\mathbf{s}^n_{CF}\times](\mathbf{G}^n_1\delta\boldsymbol{\eta}^n_{ns} + \mathbf{G}^n_2\delta\boldsymbol{\varphi})}{((x^n)^2 + (y^n)^2 + F^2)^{1/2}},$$

$$\mathbf{b} = -\mathbf{K}\sum_{n=1}^{N_S}\frac{[\mathbf{s}^n_{CF}\times]\mathbf{G}^n_3}{((x^n)^2 + (y^n)^2 + F^2)^{1/2}}\delta\mathbf{p};$$

$\mathbf{G}^n_1$, $\mathbf{G}^n_2$, $\mathbf{G}^n_3$ are matrices from (9) calculated for a star with number n = 1… N_S. The covariance matrices of the star tracker error components are given as

$$\mathbf{P}_{\mathbf{b}} = \langle\mathbf{b}\mathbf{b}^{\mathsf{T}}\rangle = \mathbf{K}\left(\sum_{n=1}^{N_S}\frac{[\mathbf{s}^n_{CF}\times]\mathbf{G}^n_3\mathbf{P}_{\delta\mathbf{p}}\mathbf{G}^{n\mathsf{T}}_3[\mathbf{s}^n_{CF}\times]^{\mathsf{T}}}{(x^n)^2 + (y^n)^2 + F^2)}\right)\mathbf{K},$$

$$\mathbf{P}_{\boldsymbol{\varepsilon}} = \langle\boldsymbol{\varepsilon}\boldsymbol{\varepsilon}^{\mathsf{T}}\rangle = \mathbf{K}\left(\sum_{n=1}^{N_S}\frac{[\mathbf{s}^n_{CF}\times](\mathbf{G}^n_1\mathbf{P}^n_{ns}\mathbf{G}^{n\mathsf{T}}_1 + \sigma^2_{\varphi}\mathbf{G}^n_2\mathbf{G}^{n\mathsf{T}}_2)[\mathbf{s}^n_{CF}\times]^{\mathsf{T}}}{(x^n)^2 + (y^n)^2 + F^2}\right)\mathbf{K}, \qquad (12)$$

where $\mathbf{P}_{\delta\mathbf{p}}$ is the covariance matrix of the errors in the values of intrinsic parameters calculated as a result of calibration. Matrices $\mathbf{P}_{\mathbf{b}}$ and $\mathbf{P}_{\boldsymbol{\varepsilon}}$ depend on the configuration of the stars in the observed constellation.

The interpretation of formulas (12) depends on how the star tracker is used in the navigation system. If it is used as an independent sensor, then (12) describes the error of a separate attitude measurement with the covariance matrix $\mathbf{P}_{\boldsymbol{\theta}} = \mathbf{P}_{\mathbf{b}} + \mathbf{P}_{\boldsymbol{\varepsilon}}$. If the star tracker measurements are used in a tightly coupled astronavigation system, which, in addition to the attitude parameters, estimates the error model's parameters of the star tracker, then (12) can be rewritten in the form of an observation equation:

$$\boldsymbol{\theta} = \mathbf{H}_{\delta\mathbf{p}}\,\delta\mathbf{p} + \boldsymbol{\varepsilon},$$

where $\mathbf{H}_{\delta\mathbf{p}} = -\mathbf{K}\sum_{n=1}^{N_S}\frac{[\mathbf{s}^n_{CF}\times]\mathbf{G}^n_3}{((x^n)^2 + (y^n)^2 + F^2)^{1/2}}$ is a matrix block of size 3×5 through which the error vector $\delta\mathbf{p}$ is observed; ε is the observation noise with the covariance matrix $\mathbf{P}_{\boldsymbol{\varepsilon}}$. Vector $\delta\mathbf{p}$ is part of the error vector of the prior estimate of the coupling filter state vector.

4. EXPERIMENTAL VERIFICATION OF THE ERROR MODEL

The error model of the star tracker was tested on experimental data obtained during ground-based calibration of the camera [32]. The calibration process consisted of six independent observation sessions, each lasting approximately 1 hour. The camera was rigidly attached to a ground base; the directions of its optical axis did not coincide with each other in different sessions. In one of the sessions, the optical axis of the camera was directed to the zenith (zenith session). In that case, the errors in correction for atmospheric refraction were close to zero.

Observation conditions in all sessions made it possible to consistently detect and identify 50–60 individual stars of magnitude 4–7 in each frame. An image composed of the brightness centers of all stars from all frames of the zenith session is shown in Fig. 2.

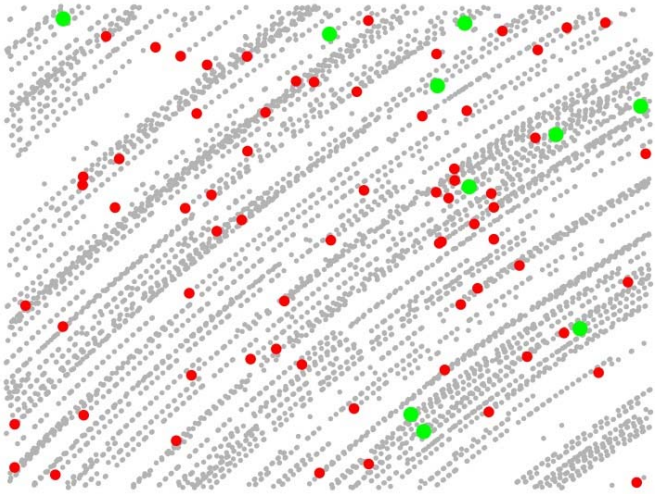

Fig. 2. Images of the brightness centers of all stars detected and identified in the zenith session (grey spots). Red spots are the brightness centers of the stars identified in the first frame; green circles are the 10 brightest stars of the first frame.

The experiment was carried out in the suburbs; in our calculations, the brightness of the optical background of the clear night sky was taken to be $m^{bg} = 21^{\text{m}}/\text{arcsec}^2$, which corresponds to the 4th level of light pollution of the sky on the scale [33]. With this method of specifying the brightness of the night sky, the standard deviation of the optical background can be written as follows:

$$\sigma_{ob} = \sqrt{T_E \times \Omega_{pix} \times P_{\text{e}}^V \times 10^{-\frac{m^{ob} - m^V}{2,5}}},$$

$$\Omega_{pix} = \left(\frac{a}{F} \times \frac{180^\circ}{\pi} \times 3600 \right)^2,$$

where Ω_{pix} is the solid angle of the pixel [arcsec^2]; m^V, P_{e}^V is the magnitude and the power of the reference star. The energy characteristics of the experimental camera and observation conditions are given in Table 1. In this table, the energy units (J and W = J/s) are converted to the number of electrons (e– and e–/s) in the charge well of the photodetector cell [28].

Individual values of vectors of calibrated intrinsic parameters were calculated for each session. The residuals of the calibration measurements served as indicators of the calibration quality:

$$\delta\boldsymbol{\xi}_{res}^n = [\delta x_{res}^n \quad \delta y_{res}^n]^{\text{T}} = \boldsymbol{\xi}^n - \boldsymbol{\xi}_{ctl}^n,$$

where $\boldsymbol{\xi}^n$ are the vector coordinates of the star n image brightness center; $\boldsymbol{\xi}_{ctl}^n$ are the vector coordinates of the same star projection onto the MPD plane calculated from the stellar catalog. The standard deviation of the residuals calculated for all stars of all frames separately for each calibration session was 0.2 pixel or 1.4 arcsec. The closeness of the standard deviations of the residuals in different sessions is the reason why we should consider all six values of the calibrated vector equally: any of these vectors can turn out to be true during the star tracker operation.

Table 1.
Energy characteristics in the experiment

Parameter	Designation	Value
Focal length	F	106.0 mm
Linear dimension of pixel	a	3.45 μm
Angular dimension of pixel	a/F	6.7 arcsec
Solid dimension of pixel	Ω_{pix}	45.1 arcsec^2
Exposure time	T_E	0.2 s
Standard deviation of readout noise	σ_{rd}	2.7 e–
Dark current	i_{dc}	46.1 e–/s
Quantization interval	QS	40.4 e–
Standard deviation of star jitter	σ_{sh}	2.1 arcsec
Brightness of the optical background	m^{bg}	21.0$^{\text{m}}$/arcsec^2
Standard deviation of the optical background	σ_{ob}	0.1 e–
Brightness of the reference star	m^V	0.03$^{\text{m}}$
Power output of the reference star	P_{e}^V	1.52×10^6 e–/s

Along with "useful" intrinsic parameters, the following "interfering" parameters were determined during the calibration process: three angles of camera attitude at the instants of each frame shooting. In this calculation, these angles are considered as the camera "true" attitude angles, and they were used to calculate the "true" matrix $\breve{\mathbf{S}}_{CF}^{GCRS}$. The vector calibrated in the zenith session is taken as "true" vector $\breve{\mathbf{p}}$ of intrinsic parameters. To simulate the calibration error, we used a "biased" vector $\mathbf{p}$ obtained by averaging the calibration results over all six sessions. The calibration error vector represented in relative units has the form:

$$(\delta\mathbf{p} / \breve{\mathbf{p}}) \times 100\% =$$

$$= [-0.0021\% \quad 0.1224\% \quad -0.0319\% \quad -1.2823\% \quad 39.0162\%]^{\text{T}}.$$

To analyze the fluctuation errors of the star tracker, all vectors $\delta\boldsymbol{\xi}_{res}^n$ obtained in all frames of the zenith session were arranged in increasing order of catalog star magnitudes m^n. The graph in Fig. 3*a* shows the result, where the residuals corresponding to the brightest stars (low magnitudes) are located on the left, and the faintest stars (high magnitudes), on the right. Superimposed on the graphs in Fig. 3*a* are the

values of the root-mean-square fluctuation errors in determining vector coordinates $\sigma^n_{ns} = \sqrt{\mathbf{P}^n_{ns}(1,1)}$ caused by the image electronic noise and $\sigma^n_{trb} = \sqrt{\mathbf{P}^n_{ns}(1,1) + \mathbf{P}^n_{trb}(1,1)}$, which take into account the stars jitter. From the figure it is clear that for a star tracker motionless inside the atmosphere, the main source of fluctuation errors is star jitters rather than electronic noise in the values of individual pixels.

The star tracker error vectors $\breve{\boldsymbol{\theta}} = [\breve{\theta}_x \ \breve{\theta}_y \ \breve{\theta}_z]^\mathsf{T}$ for the true $\breve{\mathbf{p}}$ and $\boldsymbol{\theta} = [\theta_x \ \theta_y \ \theta_z]^\mathsf{T}$ for the biased $\mathbf{p}$ vectors are restored from the expressions:

$$[\breve{\boldsymbol{\theta}}\times] \approx \mathbf{I}_3 - \mathbf{S}^{GCRS}_{CF}(\breve{\mathbf{p}})(\breve{\mathbf{S}}^{GCRS}_{CF})^\mathsf{T},$$
$$[\boldsymbol{\theta}\times] \approx \mathbf{I}_3 - \mathbf{S}^{GCRS}_{CF}(\mathbf{p})(\breve{\mathbf{S}}^{GCRS}_{CF})^\mathsf{T},$$

where $\mathbf{S}^{GCRS}_{CF}(\breve{\mathbf{p}})$, $\mathbf{S}^{GCRS}_{CF}(\mathbf{p})$ are the star tracker attitude matrices obtained from Wahba's problem solution for the same stars in the same frame, but with different intrinsic parameters. Vector $\breve{\boldsymbol{\theta}}$ contains only the fluctuation component of the error, and vector $\boldsymbol{\theta}$ has additional bias $\mathbf{b}$.

The graphs of vector $\breve{\boldsymbol{\theta}}$ components are shown in Fig. 3*b*. Bold blue lines indicate graphs of errors in the attitude calculation based on all stars recognized in the frame ($Ns \geq 50$); light blue lines indicate the errors in using the first 3...10 brightest stars for the attitude calculation. Superimposed on the error graphs are the graphs of the standard deviations $\sigma_{\breve{\theta}_x} = \sqrt{\mathbf{P}_{\boldsymbol{\theta}}(1,1)}$, $\sigma_{\breve{\theta}_y} = \sqrt{\mathbf{P}_{\boldsymbol{\theta}}(2,2)}$, $\sigma_{\breve{\theta}_z} = \sqrt{\mathbf{P}_{\boldsymbol{\theta}}(3,3)}$ calculated for $Ns = 3$ (red graph with circles) and for $Ns = 10$ (yellow graph with squares) of the brightest stars in the frame. For this number of stars, the fluctuation errors in the star tracker angles of inclination (components $\breve{\theta}_x$ and $\breve{\theta}_y$) turned out to be noticeably smaller than the error of the star tracker angle of rotation ($\breve{\theta}_z$), which is a characteristic feature of its operation [34]. A higher attitude error in the left part of Fig. 3*b* for $Ns = 3$ is due to the bad configuration of the three brightest stars in the camera field of view rather than with the convergence of some internal estimation filter.

The graphs of the modules of the attitude errors $|\breve{\boldsymbol{\theta}}|$ and $|\boldsymbol{\theta}|$ are shown in Fig. 4*a*. Bold lines indicate the error graphs when all stars identified in the frame were used to calculate the star tracker attitude; light lines show the errors in the cases when the first 3...10 brightest stars were used. Error $|\boldsymbol{\theta}|$ is entirely due to the residuals after calibration; it is the minimum error for the star tracker under consideration in real operating conditions.

The graphs of the components of vectors $\boldsymbol{\theta}$ and $\mathbf{b} = [b_x \ b_y \ b_z]^\mathsf{T}$ are shown in Fig. 4*b*. The components of vector $\boldsymbol{\theta}$ contain noise components concentrated around the components of the bias vector $\mathbf{b}$. From these graphs it is clear that in this case, the calibration errors of the intrinsic parameters have little effect on the error in determining the star tracker rotation (component b_z), but they noticeably distort the measured angles of its inclination (components b_x, b_y).

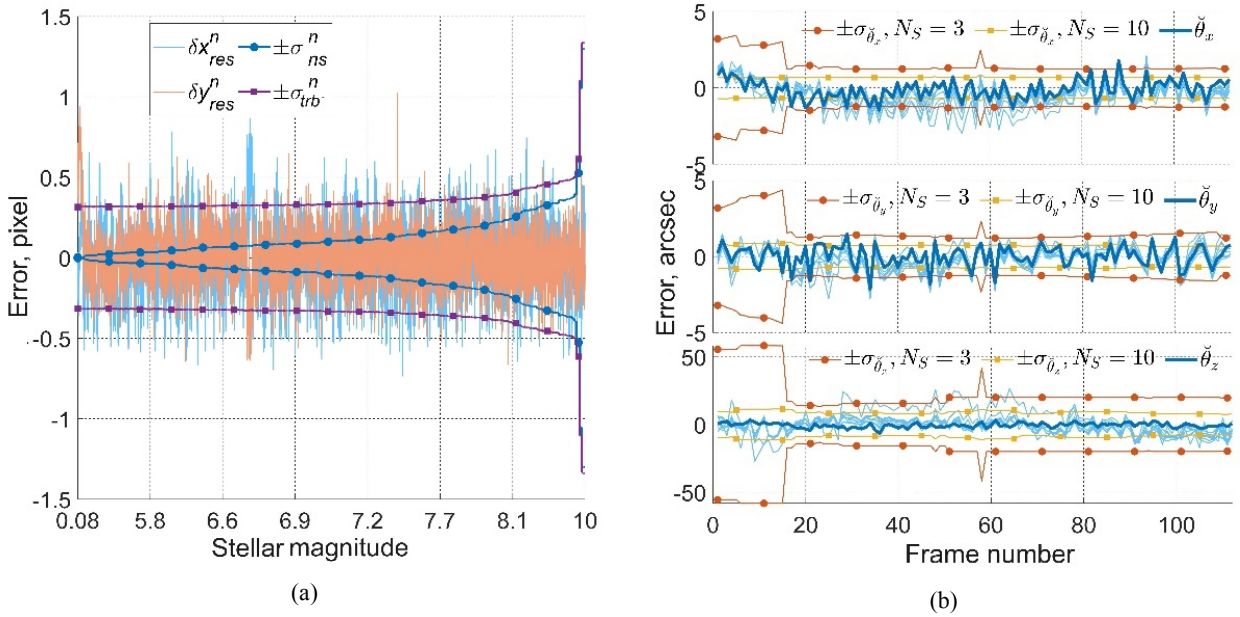

(a) (b)

Fig. 3. Fluctuation errors of the star tracker. (a) residuals after calibration of intrinsic parameters; (b) star tracker error vector components for different numbers of processed stars.

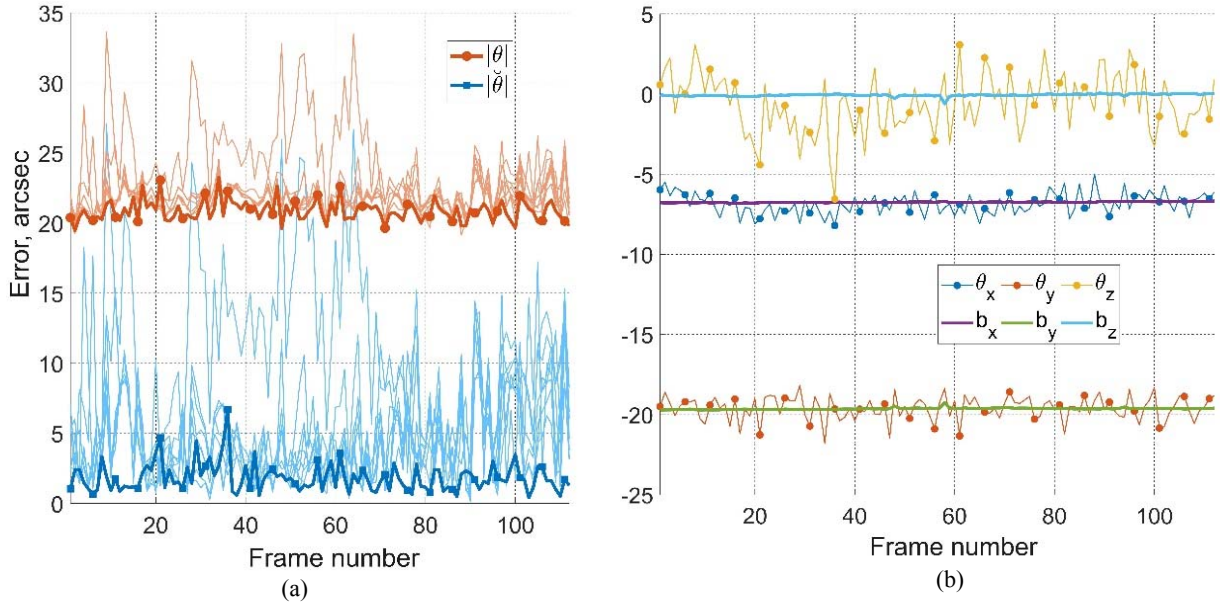

Fig. 4. The star tracker errors in the zenith session: (a) star tracker error vector magnitudes for the true and biased vectors of intrinsic parameters; (b) coordinates of the error vector and the bias vector of the star tracker.

5. CONCLUSIONS

The paper proposes a linearized model of star tracker errors which takes into account electronic noise in the digital image of stars and calibration errors of camera intrinsic parameters. For atmospheric star trackers, the model is complemented with errors in measuring apparent directions to the stars caused by atmospheric turbulence. The model does not take into account the errors associated with blurs in star images, i.e. this model can be applied in the conditions when a star tracker rotates slowly so that the angle of the field-of-view rotation does not exceed half the angular size of the pixel during the exposure time.

The experimental verification of the proposed model shows that even for a fault-free atmospheric star tracker, the values of the intrinsic parameters can significantly deviate from their values obtained during factory calibration. These deviations are small in relative magnitudes, but they lead to noticeable systematic errors in stellar attitude measurements. These errors can be eliminated by regular calibrations of intrinsic parameters during operation. If intrinsic parameters are included in the state vector of a certain estimating filter for operational calibration, the developed measurement model can be used directly to synthesize observation equations for this filter.

The values of the attitude errors measured by the star tracker may seem too small to be taken into account for the solution of practical navigation problems. In order to correctly interpret these values, we should keep in mind that the main purpose of the star tracker is not to measure attitude relative to the stars, but to obtain data to calculate the observer's position relative to the Earth. In this case, the star tracker's angular error $|\boldsymbol{\theta}|$ turns into the error of a single position measurement $|\boldsymbol{\theta}|\times R_\oplus$, where $R_\oplus \approx 6370$ km is the radius of the Earth, which is 155 m at $|\boldsymbol{\theta}| = 5$arcsec and 618 m at $|\boldsymbol{\theta}| = 20$ arcsec, i.e., from a positioning point of view, the star tracker is a very coarse navigation device compared to receivers of satellite navigation systems.

APPENDIX

PSF INTEGRATION OVER THE PHOTODETECTOR CELL AREA

To simplify the notation, we write the Gaussian PSF in the form

$$\Phi(x,y) = \frac{1}{\alpha\pi}\exp\left(-\frac{x^2+y^2}{\alpha}\right),$$

where $\alpha = 2\sigma_A^2$, $x = a(h-(\hat{h}_C+\delta h))$, $y = a(w-(\hat{w}_C+\delta w))$; $(\hat{h}_C,\hat{w}_C)$ are raster indices of the cell with the maximum PSF; δh, δw are the PSF maximum offsets relative to the upper left corner of the cell $(\hat{h}_C,\hat{w}_C)$. The signal level in a cell with raster indices $(\hat{h}_C+\hat{p},\hat{w}_C+\hat{q})$ is proportional to the integral of $\Phi(x,y)$ taken over the area of this cell:

$$\hat{\Phi}(\hat{p},\hat{q}) = \int_{a(\hat{p}-\delta h)}^{a(\hat{p}'+1-\delta h)} dx \int_{a(\hat{q}-\delta w)}^{a(\hat{q}+1-\delta w)} dy\, \Phi(x,y) =$$

$$= \frac{1}{\pi}\left[\int_{a(\hat{p}-\delta h)}^{a(\hat{p}'+1-\delta h)} e^{-\frac{x^2}{\alpha}} \frac{dx}{\sqrt{\alpha}} \times \int_{a(\hat{q}-\delta w)}^{a(\hat{q}+1-\delta w)} e^{-\frac{y^2}{\alpha}} \frac{dy}{\sqrt{\alpha}}\right].$$

After replacing the integration variables $x' = x\alpha^{-0,5}$, $y' = y\alpha^{-0,5}$, this expression is rewritten as

$$\hat{\Phi}(\hat{p},\hat{q}) = \frac{1}{4}\left[\frac{2}{\sqrt{\pi}} \int_{\frac{a(\hat{p}-\delta h)}{\sqrt{\alpha}}}^{\frac{a(\hat{p}'+1-\delta h)}{\sqrt{\alpha}}} e^{-x'^2} dx' \times \frac{2}{\sqrt{\pi}} \int_{\frac{a(\hat{q}-\delta w)}{\sqrt{\alpha}}}^{\frac{a(\hat{q}+1-\delta w)}{\sqrt{\alpha}}} e^{-y'^2} dy'\right].$$

The integrals in this product are expressed in terms of the standard error function $\mathrm{erf}(x)$:

$$\frac{2}{\sqrt{\pi}}\int_b^a e^{-x^2} dx = \mathrm{erf}\,(a) - \mathrm{erf}\,(b),\ \mathrm{erf}(x) = \frac{2}{\sqrt{\pi}}\int_0^x e^{-t^2}\, dt.$$

Hence,

$$\hat{\Phi}(\hat{p},\hat{q}) = \frac{1}{4}\left[\mathrm{erf}\left(\frac{a(\hat{p}+1-\delta h)}{\sqrt{\alpha}}\right) - \mathrm{erf}\left(\frac{a(\hat{p}-\delta h)}{\sqrt{\alpha}}\right)\right] \times$$

$$\times\left[\mathrm{erf}\left(\frac{a(\hat{q}+1-\delta w)}{\sqrt{\alpha}}\right) - \mathrm{erf}\left(\frac{a(\hat{q}-\delta w)}{\sqrt{\alpha}}\right)\right].$$

FUNDING

This work was supported by ongoing institutional funding. No additional grants to carry out or direct this particular research were obtained.

CONFLICT OF INTEREST

The author of this work declares that he has no conflicts of interest.

REFERENCES

1. Avanesov, G.A., Bessonov, R.V., Kurkina, A.N., Mysnik, E.A., Liskiv, A.S., Lyudomirskii, M.B., Kayutin, I.S., and Yamshchiko,v N.E., Development of an autonomous strapdown astroinertial navigation system, *Mekhanika, upravlenie i informatika*, 2013, no. 1(13), pp. 9–29.
2. Stepanov, O.A. and Koshaev, D.A., Studying the methods for solving the orientation problem using satellite systems, *Giroskopiya i navigatsiya*, 1999, no. 2(25), pp. 30–55.
3. Shuster, M.D. and Oh, S.D., Three-axis attitude determination from vector observations, *Journal of Guidance and Control*, 1981, vol. 4, no. 1, pp. 70–77. DOI: 10.2514/3.19717.
4. Markley, F.L., Attitude determination using vector observations and the singular value decomposition, *Journal of the Astronautical Sciences*, 1988, vol. 36, no. 3, pp. 245–258.
5. Markley, F.L. and Crassidis, J.L., *Fundamentals of Spacecraft Attitude Determination and Control,* New York: Springer, 2014. DOI 10.1007/978-1-4939-0802-8.
6. Golovan, A.A., Morgunova, S.N., Solov'ev, I.V., and Shatskii, M.A., Decomposed algorithm for the spacecraft attitude estimation in stellar correction mode. *Gyroscopy and Navigation*, 2022, vol. 13, pp. 232–240. DOI: https://doi.org/10.1134/S207510872204006X
7. Ivonin, A.N., Kamal'dinova, R.A., Morgunova, S.N., Sokolov, V.N., Solov'ev, I.V. and Shatskii, M.A., Algorithm for Spektr-UF spacecraft attitude estimation for the mode of precision guidance of telescope axis, *Aviakosmicheskoe priborostroenie,* 2020, no. 12, pp. 13–25.
8. Cheng, Y., Crassidis, J.L., and Markley, F.L., Attitude estimation for large field-of-view sensors. *The Journal of the Astronautical Sciences*, 2006, vol. 54, no. 3&4, pp. 433–448. DOI: 10.1007/BF03256499.
9. Vasilyuk, N.N., Vector correction of velocity aberration for an intra-atmospheric stellar orientation sensor, *Aviakosmicheskoe priborostroenie,* 2022n no. 10, pp. 17–31. DOI 10.25791/aviakosmos.10.2022.1302.
10. Vasilyuk, N.N., Vector correction of atmospheric refraction for an intra-atmospheric stellar orientation sensor, *Aviakosmicheskoe priborostroenie,* 2022, no. 9, pp. 31–44. DOI 10.25791/aviakosmos.9.2022.1299.
11. Solovyev I.V. Detection and estimation of star image coordinates in celestial orientation sensors using prediction and Kalman filtering algorithms, *Mekhatronika, avtomatizatsiya, upravlenie*, 2013, no. 11, pp. 59–63.
12. Tuchin, M., Biryukov, A., Nickiforov, M., Prokhorov, M., and Zakharov A., On random and systematic errors of a star tracker, 2013, *Proc. 27th AIAA/USU Conference on Small Satellites, Advanced Technologies* I, SSC13-I-10. https://digitalcommons.usu.edu/smallsat/2013/all2013/52/
13. Garanin, S.G., Zykov, L.I., Klimov, A.N., Kulikov S.M., Smyshlyaev, S.P., Stepanov, V.V., and Syundyukov, A.Yu., Daytime observation of low-brightness stars of (7^m-8^m) from flat terrain, *J. Optical Journal*, 2017, vol. 84, no. 12, pp. 816–821. https://doi.org/10.1364/JOT.84.000816
14. Lukin, V.P. and Nosov, V.V., Measurement of image jitter of an extended incoherent radiation source, *Quantum Electronics,* 2017, vol. 47, no. 6, pp. 580–588. DOI: https://doi.org/10.1070/QEL16
15. Smetanin, P.S., Avanesov, G.A., Bessonov, R.V., Kurkina, A.N., and Nikitin A.V., Geometric calibration of a high-precision star tracker using the stellar sky, *Sovremennye problemy distantsionnogo zondirovaniya Zemli iz kosmosa* (Modern Problems of Earth Remote Sensing from Space), 2017, vol. 14, no. 2, pp. 9–23. DOI 10.21046/2070-7401-2017-14-2-9-23.
16. Bazina, E.A., Bessonov, R.V., Brysin, N.N., Nikitin, A.V., Prokhorova, S.A., Slivko, N.A., Stroilov, N.A., and Yumatov, B.A., Mathematical model of a bench for determining intrinsic orientation elements, *Sovremennye problemy distantsionnogo zondirovaniya Zemli iz kosmosa* (Modern Problems of Earth Remote Sensing from Space), 2018, vol. 15, no. 6. pp. 131–144. DOI 10.21046/2070-7401-2018-15-6-131-144.
17. Chen, Z., Zheng, Y., Zhan, Y., Li, C., Chen, B., and Zhang, H., Distortion model of star tracker on-orbit calibration algorithms based on interstar angles, *Jour-*

nal of Physics: Conference Series. 2022, vol. 2235, 0120533. DOI 10.1088/1742-6596/2235/1/012053.
18. Chen, X., Xing, F., You, Z., Zhong, X., and Qi, K., On-orbit high-accuracy geometric calibration for remote sensing camera based on star sources observation, *IEEE Trans. Geoscience and Remote Sensing*, 2022, vol. 60, pp. 1–11. DOI: 10.1109/TGRS.2021.3100841.
19. Enright, J., Jovanovic I., and Vaz, B., Autonomous recalibration of star trackers, *IEEE Sensors Journal*, 2018, vol. 18, no. 18, pp. 7708–7720. DOI: 10.1109/JSEN.2018.2857621.
20. Fedoseev, V.I. and Kolosov, M.P., *Optiko-elektronnye pribory orientatsii i navigatsii kosmicheskikh apparatov* (Optoelectronic devices for reference attitude control and navigation of spacecraft). Moscow: Logos, 2007.
21. Avanesov, G.A., Kondrat'eva, T.V., and Nikitin, A.V., Study of the displacement of the energy center of star images relative to the geometric center on the CCD matrix and correction of methodological errors, *Mekhanika, upravlenie i informatika*, 2009. No. 1, pp. 421–446.
22. Brown, D.C., Decentering distortion of lenses, *Photogrammetric engineering and remote sensing*, 1966, vol. 32, no. 3, pp, 444–462.
23. Lobanov, A.N., *Fotogrammetriya: Uchebnik dlya vuzov* (Photogrammetry: Textbook for Universities), 2nd ed., rev., Moscow, Nedra, 1984.
24. Baranov, P.S. and Mantsvetov, A.A., Optimization of the ratio of the lens scattering circle radius to the pixel size to improve the estimation accuracy of the coordinates of small-sized object images, *Izvestiya vysshikh uchebnykh zavedenii Rossii. Radioelektronika*, 2016, no. 2, pp. 49–53.
25. Zakharov, A.I. and Nikiforov, M.G., Systematic and random errors in determining the positions of photocenters of stars on matrix photodetectors, *Mekhanika, upravlenie i informatika*, 2011, no. 2, pp. 280–288.
26. Stroilov, N.A., Kuptsov, T.V., Bazina, E.A., Nikitin, A.V., El'yashev, Ya.D., and Yumatov, B.A., Determination of the point-spread function of the star tracker optical system, *Sovremennye problemy distantsionnogo zondirovaniya Zemli iz kosmosa* (Modern Problems of Earth Remote Sensing from Space), 2022, vol. 19, no. 6, pp. 41–49. DOI 10.21046/2070-7401-2022-19-6-41-49.
27. Vasilyuk, N.N., Synthesis of a rotational blur kernel in a digital image using measurements of a triaxial gyroscope, *Komp'yuternaya optika*, 2022, vol. 46, no. 5, pp. 763–773. DOI 10.18287/2412-6179-CO-1081.
28. Vasilyuk, N.N., Correction of rotational blur in images of stars observed by an astroinertial attitude sensor against the background of the daytime sky, *Komp'yuternaya optika*, 2023, vol. 47, no. 1, pp. 79–91. DOI 10.18287/2412-6179-CO-1141.
29. Avanesov, G.A., Stroilov, N.A., Filippova , O.V., Shamis, V.A., and El'yashev, Ya.D., Photometric model of a star orientation sensor, *Sovremennye problemy distantsionnogo zondirovaniya Zemli iz kosmosa* (Modern Problems of Earth Remote Sensing from Space), 2019, vol. 16, no. 5, pp. 75–84. DOI 10.21046/2070-7401-2019-16-5-75-84.
30. Biryukov, A.V., Zakharov, A.I., Krusanova, N.L., Mironov, A.V., Moshkalev, V.G., Nikolaev, F.N., Prokhorov, M.E., and Tuchin, M.S., Calculation of the star brightness in the spectral band of a silicon photodetector of a star tracker based on the Tycho-2 and 2MASS catalog data, *Mekhanika, upravlenie i informatika*, 2013, no. 1(13), pp. 243–248.
31. ESA, 1997, The Hipparchos and Tycho catalogues, ESA SP-1200.
32. Vasilyuk, N.N., Nefedov, G.A., Sidorova, E.A., and Shagimuratova, N.O., Calibration of the intrinsic parameters of the digital camera of a star tracker based on ground-based observations of stars, taking atmospheric refraction and aberration of light into account, *Measurement Techniques*, 2024, vol. 66, no.,8, pp.593-609 DOI:10.1007/s11018-023-02272-z
33. Bortle, J.E., Introducing the Bortle Dark-Sky Scale, *Sky & Telescope*, 2001, vol. 101, pp. 126–138.
34. Vasilyuk N.N., Geometric accuracy limitations on a vector orientation sensor built on a matrix optical image receiver, *Aerokosmicheskoe priborostroyenie*, 2011, no. 6, pp. 17–24.